ADVANCED MATERIALS
www.advmat.de

Boosting the Power Conversion Efficiency of Perovskite Solar Cells Using Self-Organized Polymeric Hole Extraction Layers with High Work Function

Kyung-Geun Lim, Hak-Beom Kim, Jaeki Jeong, Hobeom Kim, Jin Young Kim, and Tae-Woo Lee**

Methylammonium lead halide perovskites have been intensively studied[1–9] as promising photoabsorption and carrier transporter materials in solar cells because of their excellent semiconducting properties,[10,11] broad range of light absorption, and high extinction coefficient.[5,12] Hybrid solar cells with 10.9% power conversion efficiency have been fabricated using a meso-superstructured organometal halide perovskite, which triggered a lot of attention in the solar cell research community;[5] the perovskite layer acts as both the light harvester and the hole conductor in the devices.[13] The bandgap of perovskites can be easily adjusted by incorporating metal cations,[14] inorganic anions,[15] or organic ligands.[10] Methylammonium lead halide perovskites also have the advantage of low-temperature (ca. 100 °C) solution processibility. Because of all these advantages, the power conversion efficiencies (PCEs) of perovskite-based solar cells have reached 15.4% in a solar cell that incorporates a vacuum-deposited perovskite layer and a TiO_2 layer.[6] Although the PCE of perovskite solar cells has been increased remarkably, few reports[7,16,17] have considered solution-processed planar heterojunction (SP-PHJ) structure solar cells without using a mesoporous or compact semiconducting metal oxide (e.g., TiO_2) layer processed by high-temperature sintering, and the SP-PJH solar cells to date have shown lower PCE than those with a mesoporous or compact TiO_2 layer.[3,4,6]

Commercialization of perovskite solar cells requires easy, scalable, and low-temperature methods to fabricate them efficiently by solution processing without sintering. The first solution-processed perovskite/acceptor SP-PHJ solar cell showed 3.9% PCE; it used indium tin oxide (ITO) as the positive electrode and poly(3,4-ethylenedioxythiophene):poly(styrenesulfonate) (PEDOT:PSS) as the hole extraction layer (HEL).[16] Subsequent SP-PHJ thin-film solar cells achieved PCE = 9.8% on a glass substrate and >6.4% on flexible polymer substrates; in these cells perovskite was sandwiched between the solution-processed HEL and an acceptor ([6,6]-phenyl-C_{61}-butyric acid methyl ester, PCBM).[18] More recently, high-efficiency PHJ perovskite solar cells (PCE = 12%) have been fabricated using vacuum deposition.[19]

To improve the device efficiency of SP-PHJ solar cells, interfacial engineering at electrodes is of prime importance because the interface between a photoactive layer and electrodes significantly influences both built-in potential and charge carrier extraction.[20–22] Several different HELs on top of an ITO electrode such as metal oxides (e.g., NiO_x,[23] IrO_x,[24] WO_3,[25] V_2O_5,[26] MoO_3,[26] thin insulating polymers (e.g., polytetrafluoroethylene),[27] and conducting polymers (e.g., PEDOT:PSS[28] and poly(diphenylamine))[29] have been exploited to increase PCE in organic photovoltaic devices. The same approach can be used for solution-processed perovskite/acceptor PHJ solar cells[7,16–21] because the device structures are almost the same as organic photovoltaic devices except for the photoactive layer. NiO_x has been used to increase PCE of SP-PHJ perovskite solar cells, but they require high-temperature annealing at 300 °C.[17]

PEDOT:PSS can also be considered as a good HEL because of its simple solution processibility, planarization effect on the underlying ITO layer, and a low-temperature annealing process. Therefore, the PEDOT-PSS HEL is appropriate to realize flexible SP-PHJ perovskite solar cells on flexible plastic substrates. However, the work function *WF* of PEDOT:PSS (4.9–5.2 eV depending on the ratio of PEDOT to PSS) is lower than the ionization potential *IP* of perovskite (e.g., 5.4 eV for methylammonium lead iodide ($CH_3NH_3PbI_3$)), so the potential energy loss at the PEDOT:PSS/perovskite interface decreases the built-in potential in perovskite solar cells. Clearly, a promising strategy to increase built-in potential and thereby achieve high PCE of perovskite solar cells is to use a polymeric HEL with a high *WF* that matches the *IP* of the perovskite layer.

The *WF* in HELs can be tuned by using molecular surface engineering to control the surface composition in HEL films, which depends on the molecules that are enriched at the surface and their concentration relative to the conducting polymer.[30,31] These approaches to controlling the molecules that are enriched at the surface in HELs will be very useful to determine the effect of HELs on energy level alignment at the interface. Thus we used a self-organized HEL (SOHEL), which is composed of a conducting polymer (e.g., PEDOT:PSS) and a perfluorinated ionomer (PFI), that is, tetrafluoroethylene-perfluoro-3,6-dioxa-4-methyl-7-octene-sulfonic acid copolymer. As a result of self-organization, the PFI becomes enriched on the film surface and thus can increase the surface *WF*. This implies

K.-G. Lim, H. Kim, Prof. T.-W. Lee
Department of Materials Science and Engineering
Pohang University of Science
and Technology (POSTECH)
San 31 Hyoja-dong, Nam-gu, Pohang,
Gyungbuk 790–784, Republic of Korea
E-mail: twlee@postech.ac.kr
H.-B. Kim, J. Jeong, Prof. J. Y. Kim
Department of Energy Engineering
Ulsan National Institute of Science and Technology (UNIST)
Ulsan 689–798, Republic of Korea
E-mail: jykim@unist.ac.kr

DOI: 10.1002/adma.201401775

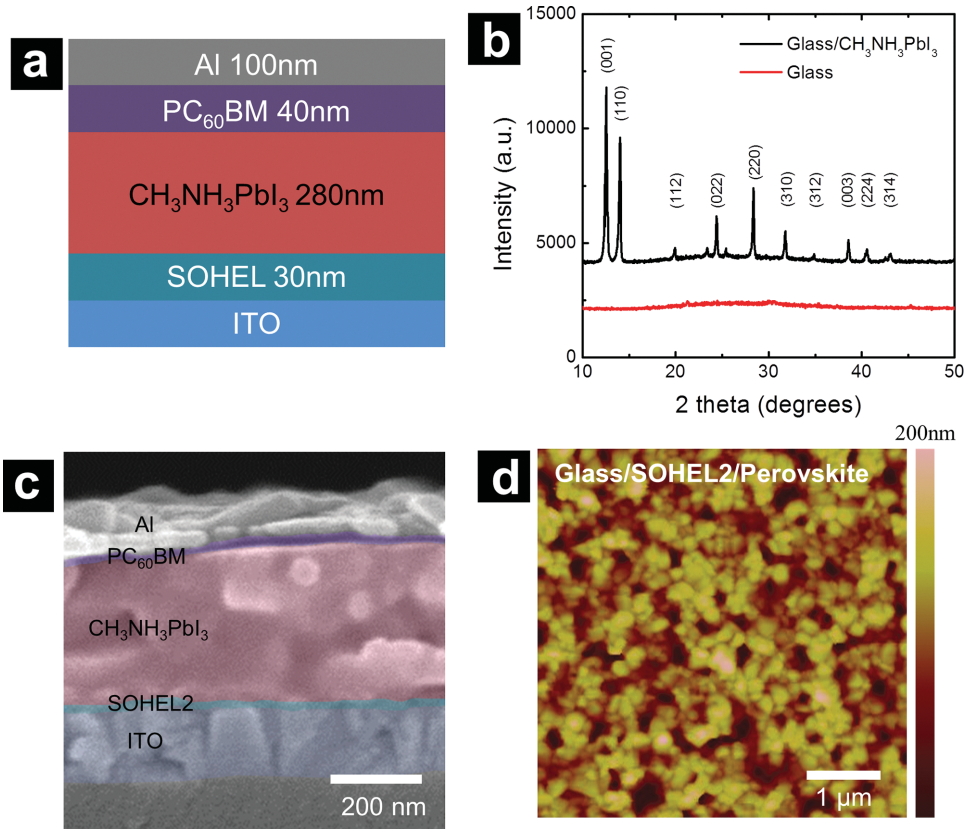

Figure 1. a) Configuration of the solar cell in this study. b) XRD patterns of the glass/$CH_3NH_3PbI_3$ and bare glass substrate. c) Cross-sectional SEM image of the optimized device configuration. The layers are tinted with the same colors as used in (a). d) AFM topography of the perovskite surface.

that the potential energy loss at the PEDOT:PSS/perovskite interface can be greatly reduced by using the high *WF* of the SOHEL, which is designed to match the *IP* levels of perovskite.

Here, we present solution-processed $CH_3NH_3PbI_3$-based perovskite solar cells with a high-*WF* SOHEL for good energy level alignment with the *IP* level of $CH_3NH_3PbI_3$. The SOHEL at the hole extraction interface can increase the built-in potential, the photocurrent, and thus the PCE of perovskite solar cells. We obtained a high PCE of 11.7% in SP-PHJ perovskite solar cells under 100 mW cm^{-2} illumination. We also demonstrated flexible perovskite solar cells on a poly(ethylene terephthalate) (PET) substrate; they had a PCE as high as 8.0%.

We prepared SOHELs (i.e., high-*WF* conducting polymer compositions) composed of highly conductive PEDOT:PSS (1:2.5 by weight, Clevios PH) and PFI (5 wt%, Sigma-Aldrich Inc.). The PFI/PEDOT:PSS weight ratios of the SOHELs are 0.105 (SOHEL1), 0.209 (SOHEL2), and 0.417 (SOHEL3). The device (**Figure 1**a) has the structure ITO/SOHEL (30 nm)/$CH_3NH_3PbI_3$ perovskite (280 nm)/PCBM (40 nm)/Al, in which all layers between electrodes were formed by spin-coating. A two-step technique for preparing $CH_3NH_3PbI_3$ films using a solution process was used to obtain surfaces that are more uniform than those prepared using one-step spin-coating.[32] First, PbI_2 films were spin-coated onto the HEL from 17.2 wt% PbI_2 solution in anhydrous *N,N*-dimethylformamide (DMF), then CH_3NH_3I was spin-cast from 20 mg mL^{-1} CH_3NH_3I solution in anhydrous isopropyl alcohol (IPA). To shorten the growth time of perovskite in the two-step process, we deposited CH_3NH_3I solution on the PbI_2 surface by spin-coating instead of dipping. The film immediately darkened after CH_3NH_3I solution casting. X-ray diffraction (XRD) patterns of glass/$CH_3NH_3PbI_3$ were in good agreement with the crystalline structure of previously reported $CH_3NH_3PbI_3$ perovskite film (Figure 1b);[16] the XRD pattern of the bare glass substrate does not show any crystal structure.

The cross-sectional image of the ITO/SOHEL/$CH_3NH_3PbI_3$ perovskite/PCBM/Al device was obtained by scanning electron microscopy (SEM, Figure 1c). The topography of the $CH_3NH_3PbI_3$ surface on the SOHEL2 was visualized using atomic force microscopy (AFM, Figure 1d); the root-mean-squared roughness R_q of the $CH_3NH_3PbI_3$ surface on the PEDOT:PSS layer and the SOHEL was 42 nm and 39 nm, respectively (Figure S1, Supporting Information).

We used ultraviolet photoelectron spectroscopy (UPS) to measure the *WF*s of the SOHELs (**Figure 2**a). Addition of PFI caused the *WF* of HELs to increase from 4.86 eV (pristine PEDOT:PSS) to 5.39 eV (SOHEL2). According to our previous density functional theory calculations,[33] the calculated *IP* of fluorinated alkyl sulfonic acid is higher than that of hydrocarbon alkyl sulfonic acid because the electron-withdrawing ability of fluorine atoms makes oxidizing a fluorocarbon sulfonic acid more difficult than oxidizing its corresponding hydrocarbon sulfonic acid. Moreover, the calculated *IP* of fluorinated sulfonic acid does not change significantly when the chain length

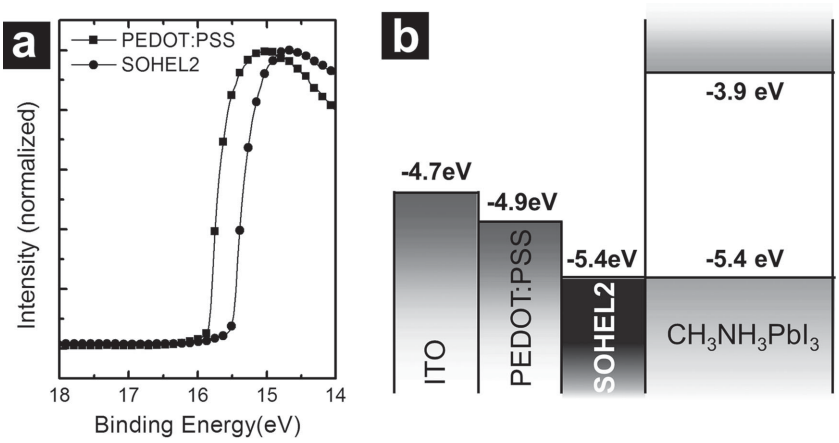

Figure 2. a) UPS of PEDOT:PSS and SOHEL2. b) Schematic of the energy levels of each layer.

is increased, whereas the *IP* of hydrocarbon alkyl sulfonic acid decreases greatly with increasing chain length. Therefore, covering the surface with the polymeric form of fluorocarbon alkyl sulfonic acid (i.e., PFI) instead of with PSS can increase the surface *WF*. We used X-ray photoelectron spectroscopy (XPS) to investigate the composition covering the SOHEL2 surface (Figure S2, Supporting Information). The C 1s core-level spectrum of the pristine PEDOT:PSS can be deconvoluted into two peaks with binding energies of 283.8, 285.3 eV (Figure S2a). The SOHEL2 also has these peaks, and two additional peaks at 290.8 and 291.3 eV, which can be assigned to fluorinated fragments of PFI at the film surface (Figure S2b). The presence of these peaks suggests that the increase in the *WF* of the SOHEL is a consequence of these fluorinated chains covering the surface. We also conducted the XPS depth profiling of PEDOT:PSS and SOHEL2 to elucidate the molecular distribution in SOHEL (Figure S3, Supporting Information). XPS depth profiling showed that the fluorocarbon chains (CF_2) in PFI molecules are enriched at the SOHEL surface and the molecular concentration of PFI gradually decreased with depth. A schematic image of the molecular distribution of PFI, PSS, and PEDOT in SOHEL2 film is given in the Supporting Information (Figure S4). We employed the HELs with various *WF*s in perovskite solar cells to clearly understand the relationship between the open-circuit voltage V_{oc} of the perovskite devices and *WF* of the HEL. We measured the *WF*s of the SOHELs versus the molecular concentration of PFI using UPS; see Figure S5a (Supporting Information). As the molecular concentration of PFI increased at the surface, the *WF*s of SOHELs also increased from 4.86 eV in pristine PEDOT:PSS to 5.46 eV in SOHEL3 (Figure S5b). The work function of SOHEL2 matches well the ionization potential level of $CH_3NH_3PbI_3$ perovskite (5.4 eV)[19] (Figure 2b); this similarity implies that the potential energy loss at the PEDOT:PSS/perovskite interface can be greatly reduced by using the SOHEL in SP-PHJ perovskite solar cells.

Current density versus voltage (*J*–*V*) characteristics of the perovskite photovoltaic cells with an ITO/HEL (PEDOT:PSS or SOHEL2)/$CH_3NH_3PbI_3$/PCBM/Al structure were obtained under irradiation with air mass (AM)-1.5 global simulated sunlight at an intensity of 100 mW cm^{-2} (**Figure 3**a). The $CH_3NH_3PbI_3$ perovskite device based on SOHEL2 (*WF* = 5.39 eV) had a higher V_{oc} (0.992 V), short-circuit current density J_{sc} (16.7 mA cm^{-2}), and fill factor *FF* (70.5%) than the device based on pristine PEDOT:PSS (*WF* = 4.9 eV) (V_{oc} = 0.835 V; J_{sc} = 14.1 mA cm^{-2}; *FF* = 68.5%) (**Table 1**, Table S1 in the Supporting Information). The device based on SOHEL2 had PCE = 11.7%, whereas the device based on pristine PEDOT:PSS had PCE = 8.1%. We investigated the device parameters and *J*–*V* curve of perovskite solar cells with PEDOT:PSS and SOHEL for various PFI/PEDOT:PSS ratios. The results are presented in Table S2 and Figure S6 (Supporting Information), respectively. The V_{oc} tended to increase steadily as a function of *WF* of HEL (Figure S7, Supporting Information).

The V_{oc} increase in the SOHEL/$CH_3NH_3PbI_3$ perovskite device can be understood by examining the schematic energy diagram (Figure 2b). V_{oc} is determined by the built-in potential V_{bi} in the devices. V_{bi} in devices using PEDOT:PSS and ITO layers is dependent on the *WF* of PEDOT:PSS rather than on the *WF* of ITO.[34] When the HEL *WF* is well aligned with the *IP* of $CH_3NH_3PbI_3$, the potential energy loss at the interface will be minimized and thus V_{bi} increases. When pristine PEDOT:PSS (*WF* = 4.9 eV) was used, the energy offset at the hole extraction interface was huge (ca. 0.5 eV) in the $CH_3NH_3PbI_3$ perovskite device. This hole extraction energy offset indicates that the PEDOT:PSS/$CH_3NH_3PbI_3$ device loses potential energy at the hole extraction interface.[35]

Owing to the good alignment of the *WF* of the SOHEL with the *IP* of the $CH_3NH_3PbI_3$ layer, the dark current of the SOHEL/$CH_3NH_3PbI_3$ devices was greatly increased compared with that of PEDOT:PSS/$CH_3NH_3PbI_3$ devices, implying that the SOHEL makes better hole injection contact. The rectification ratio (forward-biased current/reverse-biased current) at ±2.0 V in the dark *J*–*V* characteristic curve was ca. 10^3 for the device with SOHEL2, but ca. 10^2 for the device with PEDOT:PSS (Figure 3b). The external quantum efficiency (EQE) spectra of the SOHEL2/$CH_3NH_3PbI_3$ device had a value of 72% at the maximum, whereas that of the PEDOT:PSS/$CH_3NH_3PbI_3$ device was 61% (Figure 3c). The energy value calculated from the onset wavelength at which the generation of photocurrent started (799 nm) was 1.55 eV, which is in good agreement with the bandgap of the $CH_3NH_3PbI_3$ (1.5 eV). The UV-vis absorption extended over the complete visible spectrum up to 800 nm, with a local maximum at ca. 500 nm, this absorption pattern indicates good formation of a $CH_3NH_3PbI_3$ perovskite layer on the glass substrate.[19] We also fabricated flexible $CH_3NH_3PbI_3$ solar cells that include SOHEL2 (Figure 3d). The device was fabricated on a ITO-coated PET substrate and it showed the high PCE (8.0%) of the flexible $CH_3NH_3PbI_3$ solar cells.[36,37]

To compare the V_{bi} of the SOHEL2/$CH_3NH_3PbI_3$ perovskite solar cells with that of the PEDOT:PSS/$CH_3NH_3PbI_3$ counterpart, we measured the net photocurrent density (i.e., the difference ΔJ of photocurrent between under illumination and in the dark) (**Figure 4**a). The compensation voltage V_0 at which $\Delta J = 0$ is correlated with V_{bi} :[38]

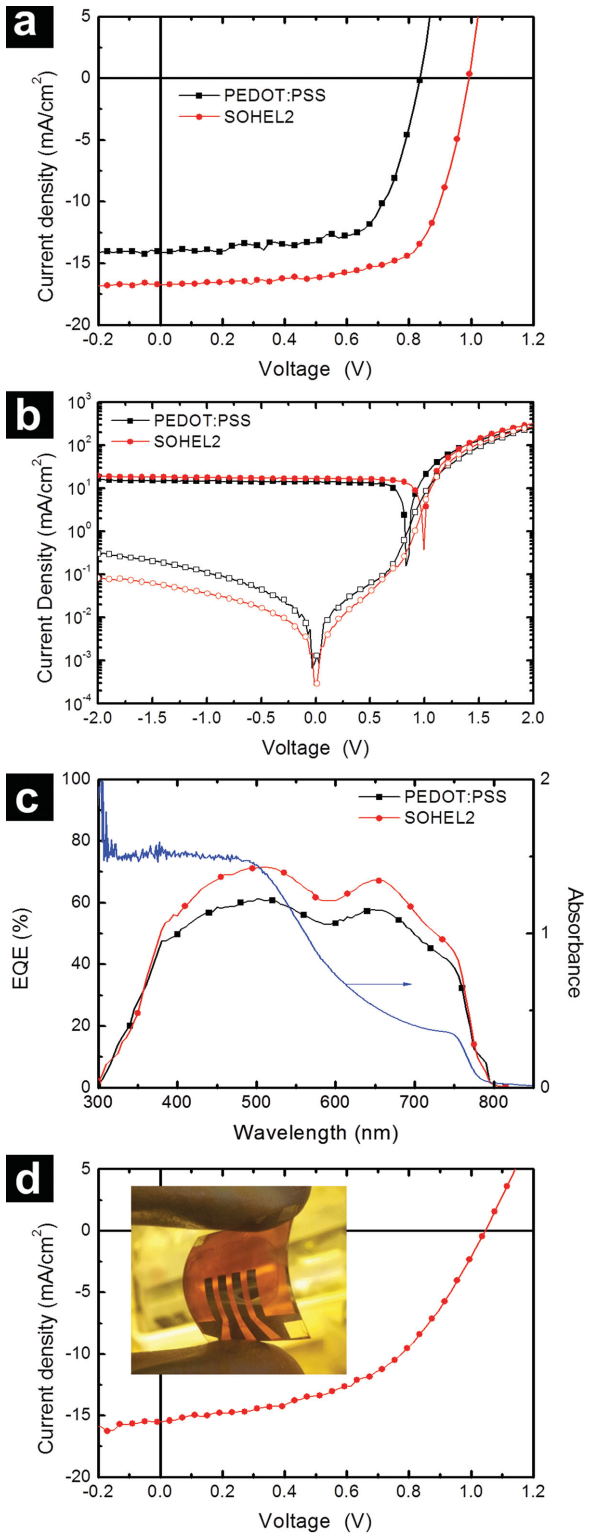

Figure 3. Photovoltaic performance characteristics. a) *J–V* curves of perovskite solar cells with PEDOT:PSS or SOHEL2 at 100 mW cm^{-2}. b) log(*J*) vs. *V* under illumination (filled symbols) and in the dark (empty symbols). (c) EQE spectra and UV-vis absorbance. d) *J–V* curves of the flexible perovskite solar cells with SOHEL2. The inset shows the photo image of flexible perovskite solar cells on PET/ITO substrate.

Table 1. Performance parameters of the perovskite solar cells with PEDOT:PSS and SOHEL2.

	V_{oc} [V]	J_{sc} [mA cm^{-2}]	*FF* [%]	*PCE* [%]	R_{sh} [Ω cm^2]	R_s [Ω cm^2]
PEDOT:PSS	0.835	14.1	68.5	8.1	1125.0	7.7
SOHEL2 (glass)	0.982	16.7	70.5	11.7	1358.4	6.9
SOHEL2 (PET)	1.040	15.5	49.9	8.0	660.0	14.5

$$V_0 = V_{bi} - \frac{k_B T}{e}\ln(A) \quad (1)$$

where k_B is the Boltzmann constant, T the absolute temperature, e the magnitude of the electron charge, and A a material parameter. The higher V_0 of the SOHEL2/perovskite device (V_0 = 1.196 V) than that of the PEDOT:PSS/perovskite device (1.019 V) is due to the increased forward diffusion of photogenerated carriers in the SOHEL2/perovskite device. This increased diffusion implies that the electric field inside the SOHEL/perovskite device (i.e., built-in potential) is higher than

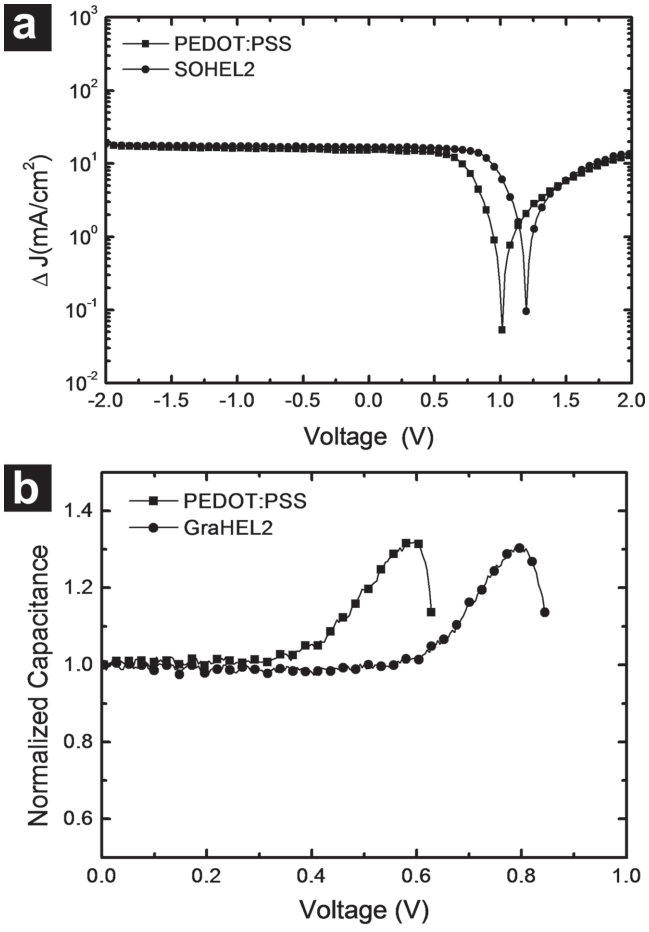

Figure 4. a) The difference of photocurrent between under illumination and in the dark (Δ*J*) vs. voltage for an ITO/SOHEL2/$CH_3NH_3PbI_3$/PCBM/Al device (circles) and an ITO/PEDOT:PSS/$CH_3NH_3PbI_3$/PCBM/Al device (squares). b) Capacitance vs. voltage plot of the devices.

inside the PEDOT:PSS/perovskite device. The compensation voltage analysis reveals high V_{bi} in the high-*WF* SOHEL/perovskite device; thus the device characteristics V_{oc}, *FF*, and J_{sc} were increased (Figure 2a,c).

We also investigated the effect of the SOHEL by measuring the capacitance–voltage (*C*–*V*) characteristics at 100 Hz (Figure 4b). The accumulated space charge inside the device can increase its capacitance. As the applied voltage increased, the capacitance tended to increase to a peak and then decrease. The V_{bi} is correlated with the voltage V_{peak} at the peak capacitance as[39]

$$V_{bi} - V_{peak} \propto \frac{k_B T}{e} \quad (2)$$

In photovoltaic devices, a higher V_{peak} implies a higher V_{bi} and thus higher V_{oc}.[30] The value of V_{peak} of SOHEL2/$CH_3NH_3PbI_3$ perovskite solar cells (0.800 V) was higher than that of the PEDOT:PSS/$CH_3NH_3PbI_3$ counterpart (0.600 V); this difference also indicates that using SOHEL2 instead of PEDOT:PSS increases the V_{bi} of the device.

In conclusion, high-*WF* SOHELs were used to achieve high PCE in SP-PHJ perovskite solar cells. A SOHEL achieves a good energy level alignment with the *IP* level of $CH_3NH_3PbI_3$ so that the SOHEL increases V_{bi}. Owing to the increased V_{bi} in the SOHEL/$CH_3NH_3PbI_3$ device, its V_{oc}, *FF*, and J_{sc} were increased. We obtained a high PCE of 11.7% under AM-1.5 global simulated irradiation of 100 mW cm^{-2}. The increase of V_0 in the net photocurrent *J*–*V* curve and the increase of V_{peak} in the *C*–*V* curve indicate that V_{bi} of the SOHEL/$CH_3NH_3PbI_3$ device increased compared with that of the pristine PEDOT:PSS/$CH_3NH_3PbI_3$ device. Our results demonstrate that interface engineering at the positive electrode in SP-PHJ perovskite solar cells by using a high-*WF* HEL is very effective to achieve high device efficiency. Because our SOHEL can be processed at low temperature, we also fabricated a flexible perovskite solar cell with SOHEL on a PET/ITO substrate; this solar cell reached a PCE as high as 8.0%.

Experimental Section

Materials and Sample Preparation: Ethylammonium lead iodide ($CH_3NH_3PbI_3$) perovskite was prepared as reported elsewhere.[15] Methylamine (CH_3NH_2) (13.5 mL, 40 wt% in aqueous solution, Alfa Aesar) and hydroiodic acid (HI) (15.0 mL, 57 wt% in water, Alfa Aesar) were stirred at 0 °C under nitrogen (N_2) atmosphere for 2 h. After the reaction, the solvent was removed using a rotary evaporator. This reaction generated a white powder, methylammonium iodide (CH_3NH_3I). The precipitate was washed with diethyl ether (Sigma-Aldrich) three times and dried at 60 °C in a vacuum oven overnight.

Device Fabrication: A solution of PEDOT:PSS (Clevios PH) was mixed with 5 wt% tetrafluoroethylene-perfluoro-3,6-dioxa-4-methyl-7-octene-sulfonic acid copolymer (a perfluorinated ionomer, PFI) (Sigma-Aldrich Co.) and spin-coated as a hole extraction layer (30 nm thick) on top of ITO/glass. The PFI/PEDOT:PSS weight ratio of the SOHELs are 0.105, 0.209, and 0.417 for the solutions of SOHEL1, 2, and 3, respectively. The SOHEL was baked on a hotplate in air at 150 °C for 10 min. The substrates were moved to a N_2 glove box, then a PbI_2 layer was spin cast from 17.2 wt% PbI_2 solution in anhydrous *N*,*N*-dimethylformamide (DMF) (Aldrich) with a spin-coating speed of 8000 rpm for 30 s, followed by thermal annealing at 70 °C for 10 min. The CH_3NH_3I was deposited from 20 mg mL^{-1} CH_3NH_3I solution in anhydrous IPA with spin-coating speed of 3000 rpm for 30 s; the film immediately darkened after the CH_3NH_3I solution was added. The coated films were then placed on a hotplate set at 100 °C for 5 min. The PCBM layer was spin-coated from 0.7 wt% PCBM (nano-C Inc.) solution in chloroform, then cathodes were thermally evaporated on the photoactive layer surface in a vacuum (2×10^{-7} Torr). A 20 nm Al cathode layer was deposited at 1 Å s^{-1} and an 80-nm Al cathode layer was deposited at 3 Å s^{-1} sequentially. The photoactive area (0.06 cm^2) was determined using metallic shadow masks. In the N_2 glove box, a UV-curable epoxy resin was used to encapsulate the devices with a glass lid.

Characterization: The current density–voltage characteristics (*J*–*V* curves) were obtained using a Keithley 2400 source measurement unit under irradiation at AM-1.5 100 mW cm^{-2} generated using a Newport 69907 solar simulator.

X-ray photoelectron spectroscopy (XPS) was conducted using a ThermoFisher / Escalab 250xi instrument with a monochromatized Al Kα source. Depth profiling with XPS was conducted to obtain the molecular profiles. The base pressure of the measurement chambers was 1×10^{10} Torr. All measurements were conducted at room temperature. The surface *WF* was measured using UPS.

The crystallographic properties of $CH_3NH_3PbI_3$ perovskite on the glass substrate were characterized using XRD (Rigaku D/MAX2500, 18 kW rotating-anode X-generator) at a scan rate of 4 °/min.

Supporting Information

Supporting Information is available from the Wiley Online Library or from the author.

Acknowledgements

This work was supported by a National Research Foundation of Korea (NRF) grant funded by the Korean government (MSIP) (NRF-2013R1A2A2A01068753 and NRF-2013R1A2A2A01015342).

Received: April 19, 2014
Revised: May 31, 2014
Published online: August 14, 2014

[1] A. Kojima, K. Teshima, Y. Shirai, T. Miyasaka, *J. Am. Chem. Soc.* **2009**, *131*, 6050.
[2] H. S. Kim, J. W. Lee, N. Yantara, P. P. Boix, S. A. Kulkarni, S. Mhaisalkar, M. Grätzel, N. G. Park, *Nano Lett.* **2013**, *13*, 2412.
[3] J. H. Heo, S. H. Im, J. H. Noh, T. N. Mandal, C. S. Lim, J. A. Chang, Y. H. Lee, H. Kim, A. Sarkar, M. K. Nazeeruddin, M. Grätzel, S. I. Seok, *Nat. Photonics* **2013**, *7*, 486.
[4] J. Burschka, N. Pellet, S.-J. Moon, R. Humphry-Baker, P. Gao, M. K. Nazeeruddin, M. Grätzel, *Nature* **2013**, *499*, 316.
[5] M. M. Lee, J. Teuscher, T. Miyasaka, T. N. Murakami, H. J. Snaith, *Science* **2012**, *338*, 643.
[6] M. Liu, M. B. Johnston, H. J. Snaith, *Nature* **2013**, *501*, 395.
[7] P.-W. Liang, C.-Y. Liao, C.-C. Chueh, F. Zuo, S. T. Williams, X.-K. Xin, J. Lin, A. K.-Y. Jen, *Adv. Mater.* **2014**, *26*, 3748.
[8] G. Hodes, *Science* **2013**, *342*, 317.
[9] G. E. Eperon, V. M. Burlakov, P. Docampo, A. Goriely, H. J. Snaith, *Adv. Funct. Mater.* **2014**, *24*, 151.
[10] C. R. Kagan, D. B. Mitzi, C. D. Dimitrakopoulos, *Science* **1999**, *286*, 945.
[11] K. Tanaka, T. Takahashi, T. Ban, T. Kondo, K. Uchida, N. Miura, *Solid State Commun.* **2003**, *127*, 619.
[12] J. H. Im, C. R. Lee, J. W. Lee, S. W. Park, N. G. Park, *Nanoscale* **2011**, *3*, 4088.
[13] L. Etgar, P. Gao, Z. Xue, Q. Peng, A. K. Chandiran, B. Liu, M. K. Nazeeruddin, M. Grätzel, *J. Am. Chem. Soc.* **2012**, *134*, 17396.

[14] D. B. Mitzi, *Chem. Mater.* **1996**, *8*, 791.
[15] G. Xing, N. Mathews, S. S. Lim, N. Yantara, X. Liu, D. Sabba, M. Grätzel, S. Mhaisalkar, T. C. Sum, *Nat. Mater.* **2014**, *13* , 476.
[16] J. Y. Jeng, Y. F. Chiang, M. H. Lee, S. R. Peng, T. F. Guo, P. Chen, T. C. Wen, *Adv. Mater.* **2013**, *25*, 3727.
[17] J.-Y. Jeng, K.-C. Chen, T.-Y. Chiang, P.-Y. Lin, T.-D. Tsai, Y.-C. Chang, T.-F. Guo, P. Chen, T.-C. Wen, Y.-J. Hsu, *Adv. Mater.* **2014**, *26*, 4107.
[18] P. Docampo, J. M. Ball, M. Darwich, G. E. Eperon, H. J. Snaith, *Nat. Commun.* **2013**, *4*, doi: 10.1038/ncomms3761.
[19] O. Malinkiewicz, A. Yella, Y. H. Lee, G. M. Espallargas, M. Grätzel, M. K. Nazeeruddin, H. J. Bolink, *Nat. Photonics* **2014**, *8*, 128.
[20] B. Cai, Y. Xing, Z. Yang, W.-H. Zhang, J. Qiu, *Energy Environ. Sci.* **2013**, *6*, 1480.
[21] N. J. Jeon, J. Lee, J. H. Noh, M. K. Nazeeruddin, M. Grätzel, S. I. Seok, *J. Am. Chem. Soc.* **2013**, *135*, 19087.
[22] Y. S. Kwon, J. Lim, H.-J Yun, Y.-H. Kim, T. Park, *Energy Environ. Sci.* **2014**, *7*, 1454.
[23] M. D. Irwin, D. B. Buchholz, A. W. Hains, R. P. H. Chang, T. J. Marks, *Proc. Natl. Acad. Sci. USA* **2008**, *105*, 2783.
[24] G. H. Jung, K. G. Lim, T.-W. Lee, J. L. Lee, *Sol. Energy Mater. Sol. Cells* **2011**, *95*, 1146.
[25] S. C. Han, W. S. Shin, M. S. Seo, D. Gupta, S. J. Moon, S. H. Yoo, *Org. Electron.* **2009**, *10*, 791.
[26] V. Shrotriya, G. Li, Y. Yao, C. W. Chu, Y. Yang, *Appl. Phys. Lett.* **2006**, *88*, 073508.
[27] B. Kang, L. W. Tan, S. R. P. Silva, *Appl. Phys. Lett.* **2008**, *93*, 133302.
[28] C.-J. Ko, Y.-K. Lin, F.-C. Chen, C.-W. Chu, *Appl. Phys. Lett.* **2007**, *90*, 063509.
[29] C.-Y. Li, T.-C. Wen, T.-F. Guo, *J. Mater. Chem.* **2008**, *18*, 4478.
[30] a) M.-R. Choi, T.-H. Han, K.-G. Lim, S.-H. Woo, D. H. Huh, T.-W. Lee, *Angew. Chem. Int. Ed.* **2011**, *50*, 6274; b) M.-R. Choi, S.-H. Woo, T.-H. Han, K.-G. Lim, S.-Y. Min, W. M. Yun, O. K. Kwon, C. E. Park, K.-D. Kim, H.-K. Shin, M.-S. Kim, T. Noh, J. H. Park, K.-H. Shin, J. Jang, T.-W. Lee, *ChemSusChem* **2011**, *4*, 363.
[31] a) J. Hwang, F. Amy, A. Kahn, *Org. Electron.* **2006**, *7*, 387; b) T.-W. Lee, Y. Chung, *Adv. Funct. Mater.* **2008**, *18*, 2246; c) T.-H. Han, Y. Lee, M.-R. Choi, S.-H. Woo, S.-H. Bae, B. H. Hong, J.-H. Ahn, T.-W. Lee, *Nat. Photonics* **2012**, *6*, 105; d) H. Kim, S.-H. Bae, T.-H. Han, K.-G. Lim, J.-H. Ahn, T.-W. Lee, *Nanotechnology* **2014**, *25*, 014012.
[32] D. Bi, S.-J. Moon, L. Häggman, G. Boschloo, L. Yang, E. M. J. Johansson, M. K. Nazeeruddin, M. Grätzel, A. Hagfeldt, *RSC Adv.* **2013**, *3*, 18762.
[33] a) T. -W. Lee, Y. Chung, O. Kwon, J. J. Park, *Adv. Funct. Mater.* **2007**, *17*, 390; b) T.-W. Lee, O. Kwon, M.-G. Kim, S. H. Park, J. Chung, S. Y. Kim, Y. Chung, J.-Y. Park, E. Han, D. H. Huh, J.-J. Park, L. Pu, *Appl. Phys. Lett* **2005**, *87*, 231106.
[34] T. M. Brown, J. S. Kim, R. H. Friend, F. Caciallia, R. Daik, W. J. Feast, *Appl. Phys. Lett.* **1999**, *75*, 1679.
[35] V. D. Mihailetchi, P. W. M. Blom, J. C. Hummelen, M. T. Rispens, *J. Appl. Phys.* **2003**, *94*, 10.
[36] J. You, Z. Hong, Y. M. Yang, Q. Chen, M. Cai, T.-B. Song, C.-C Chen, S. Lu, Y. Liu, H. Zhou, Y. Yang, *ACS Nano* **2014**, *8*, 1674.
[37] a) M. H. Kumar, N. Yantara, S. Dharani, M. Grätzel, S. Mhaisalkar, P. P. Boix, N. Mathews, *Chem. Commun.* **2013**, *49*, 11089; b) Y.-F. Chiang, J.-Y. Jeng, M.-H. Lee, S.-R. Peng, P. Chen, T.-F. Guo, T.-C. Wen, Y.-J. Hsue, C.-M. Hsu, *Phys. Chem. Chem. Phys.* **2014**, *16*, 6033; c) C. R. Carmona, O. Malinkiewicz, A. Soriano, G. Mínguez Espallargas, A. Garcia, P. Reinecke, T. Kroyer, M. I. Dar, M. K. Nazeeruddine, H. J. Bolink, *Energy Environ. Sci.* **2014**, *7*, 994; d) D. Liu, T. L. Kelly, *Nat. Photonics* **2013**, *8*, 133.
[38] G. G. Malliaras, J. R. Salem, P. J. Brock, J. C. Scott, *J. Appl. Phys.* **1998**, *84*, 1583.
[39] a) K.-G. Lim, M. R. Choi, J. H. Kim, D. H. Kim, G. H. Jung, Y. Park, J.-L. Lee, T.-W. Lee, *ChemSusChem* **2014**, *7*, 1125; b) K. G. Lim, M.-R. Choi, H.-B. Kim, J. H. Park, T. W. Lee, *J. Mater. Chem.* **2012**, *22*, 23148.